CrystEngComm

PAPER

View Article Online
View Journal | View Issue

Cite this: *CrystEngComm*, 2024, **26**, 6748

Controlling the architecture of Au/Pt core–shell nanocubes *via* platinum growth mode†

Imke Maack, [a] Kevin Oldenburg [b] and Katharina Al-Shamery *[a]

In order to overcome the often large activation barriers in heterogeneous catalytic reactions, photocatalysis is a promising path to activate specific molecules with light at moderate temperatures. In particular, bimetallic nanoparticles combining the plasmonic properties of one metal with the high catalytic activity of another are promising antenna–reactor systems. As the nanocrystal surface structure is a major factor in steering surface electronic properties and accompanying activity and selectivity, it is of interest to control the metal nanoparticle growth and composition. The subject of this work is the synthesis of gold–platinum nanoparticles with varying architectures by controlling the growth mechanism. The selection of the reducing agent allows the regulation of the reduction rate of the platinum metal salt, which in turn affects the final morphology of the resulting bimetallic nanoparticles. This allows the synthesis of either core–shell nanocrystals with decorated nanocube corners or dendritic particles under otherwise identical reaction conditions. A dendritic structure requires the rapid deposition of platinum monomers on the surface of the gold particles. This process hinders the diffusion of platinum monomers to energetically preferred sites on the particle surface, which is possible during the formation of core–shell nanocrystals.

Received 16th August 2024,
Accepted 31st October 2024

DOI: 10.1039/d4ce00823e

rsc.li/crystengcomm

Introduction

Colloidal nanoparticles are of great interest due to their wide range of applications, such as in photonics,[1,2] sensing,[3,4] or catalysis.[5–7] Precise adjustment of different parameters like particle size, shape, composition, or stabilizing ligands allows the control of the properties and thereby optimization for different purposes. In nanocrystals, like cubes, enhanced electromagnetic near fields can be generated due to their sharp features, which is why the particle shape is an important parameter for photonic applications.[8] Therefore, the synthesis of nanocubes consisting of silver,[7,9,10] palladium,[11] platinum,[12,13] or gold,[14,15] for example, has been in the focus of recent research. Directing agents such as halide ions are a key factor for the synthesis of such anisotropic nanocrystals because of their ability to block specific sites during growth. In general, halide ions have the property to chemisorb on different metal facets with different strengths in the following order $I^- > Br^- > Cl^- > F^-$.[16] In the case of gold nanocube synthesis, bromide is often used because of its ability to strongly adsorb on Au(100) facets, blocking these facets.[17] As a consequence, a higher formation rate is observed in the [111] and [110] directions compared to the [100] direction, leading to the formation of the cubic particle shape.[15] In many cases, further functionalization of the nanostructures allows the tailoring for specific applications, for example, by exchanging the particle-stabilizing ligand[18,19] or by decorating the nanoparticles with another metal. In the case of bimetallic nanoparticles, the architecture is a significant factor influencing their properties and potential applications. Depending on the growth mechanism, the nanoparticles can adopt different structures, including core–shell, core–frame, Janus structure, intermetallic, or alloy structures. In general, the nanoparticle growth can be controlled either kinetically or thermodynamically, which also influences the relationship between the deposition and diffusion of the monomers.[20–22] Monomer immobilization occurs on sites with relatively high energy gain, such as corners and edges. In contrast, diffusion takes place between facets with low energy gain. In thermodynamically controlled overgrowth, the diffusion of monomers is faster than their deposition. This results in the migration of adatoms on the nanoparticle surface and minimization of surface energy.[23] In contrast, the diffusion process in kinetically controlled overgrowth is slower than the deposition and results in the formation of structures with a higher free energy. Important parameters for this control are for

[a] *Carl von Ossietzky University of Oldenburg, Institute of Chemistry, Carl von Ossietzky St. 9-11, D-26129 Oldenburg, Germany.*
E-mail: katharina.al.shamery@uol.de
[b] *Center for Interdisciplinary Electron Microscopy (ELMI-MV), Department Life, Light, and Matter, University of Rostock, Albert-Einstein Str. 25, D-18059 Rostock, Germany*

† Electronic supplementary information (ESI) available: TEM micrographs of gold nanocubes and gold nanocubes after heating with size histograms, EDS spectra of gold–platinum nanoparticles, TEM micrographs of gold–platinum nanoparticles. See DOI: https://doi.org/10.1039/d4ce00823e

instance the reducing agent, the reaction temperature, the directing agent and the injection rate, or the pH value.[24–27] Control of the pH value enables the regulation of the reducing ability of the reducing agent, and this influences the degree of supersaturation[28] of the solution, which is important for the growth mechanism. This strategy allows precise control of the surface structure in the case of palladium–platinum core–shell nanostructures, for which palladium nanocubes are used as seed particles.[27] By varying the pH value, a change in the growth mechanism from island growth with Pt [111] facets to conformal Pt overgrowth with [100] facets occurs.[27] The effect of the reduction agent was studied, for example, in the case of palladium–gold nanoparticles.[29] Depending on whether ascorbic acid or citric acid was used, a conformal or localized overgrowth occurred. In another study, a structure change from gold–platinum core–shell to dendritic particles was observed when the injection rate was increased due to higher deposition rates.[30] Characteristic for dendritic nanomaterials is a large specific surface area due to their branches. This is important for improving catalytic activity as it can result in catalytic hotspots.[25,31] Besides these morphological properties, gold–platinum structures are of great interest for photocatalysis as the optical properties of gold are combined with the catalytical properties of platinum.

Gold nanoparticles are well known for their localized surface plasmon resonance (LSPR) in the optical spectrum.[32] With respect to catalysis, it is well-established that gold nanoparticles smaller than 10 nm typically exhibit catalytic activity.[33] By decorating the facets of larger nanocrystals with platinum, the particle's surface becomes catalytically active, and plasmonic properties can be further tuned on demand. Hence, gold–platinum core–shell nanoparticles can be used to efficiently collect light from the far-field to the catalytically active surface region to trigger photocatalytic reactions. The challenge in these hybrid plasmonic systems is the optimization of the energy flow across the plasmonic/non-plasmonic interfaces while keeping the desired plasmonic properties. Nanoparticles consisting of Au–Pt as an antenna–reactor system are of particular interest as Pt with its partially filled d-band intersecting with E_F can absorb photons *via* interband excitations in the visible range. Au on the other hand has full d-bands so that visible photons can induce direct, momentum-conserving d-to-s interband photonic excitations in a certain spectral range of the visible spectrum due to the position with respect to E_F.[1] As a consequence, plasmon decay *via* these excitations are important, exhibiting asymmetric distributions of low energy s electrons and high energy d holes.[34] Therefore, combining Au nanoparticles with Pt enables new pathways for e–h formation and surface localization available for the hybrid plasmonic system.[34]

Such processes can thus be used for chemical transformation of adsorbed molecules. Concerning the applications of nanocrystals in the field of catalysis, the reactants should adsorb strongly to the surface of the catalyst and be activated, while the product should adsorb weakly and be desorbed easily from the surface.[35] In this case, the particle shape and the resulting arrangement of surface atoms, which leads to the formation of different facets, is also important. This was demonstrated, for example, in the oxygen reduction reaction on single-crystal surfaces with perchloric acid.[36] The results show that the reaction is highest on the Pt(110) facet, followed by the Pt(111) facets, and lowest on the Pt(100) surface.[36] An increase in the activity of the oxygen reduction reaction could be achieved by modification with nickel because the $Pt_3Ni(111)$ surface has a 10-fold higher activity compared to Pt(111).[36]

In this work, we present a synthesis approach for the preparation of bimetallic gold–platinum nanocubes that allows precise control of the particle structure *via* platinum growth. By varying the reduction agent that influences the growth mode of the platinum, we can selectively synthesize either cubically shaped bimetallic nanocrystals that have a core–shell structure with decorated rounded cube corners or those with a dendritic platinum shell. These different surface morphologies are very promising for further photocatalytic applications. The nanostructures were analyzed by high-resolution transmission electron microscopy (HR-TEM) to get a detailed insight into the particle structure. Energy-dispersive X-ray spectroscopy – (EDS) measurements were performed for the elemental distribution. Moreover, the particles are characterized by UV/vis spectroscopy).

Experimental section

The following materials were used without further purification: gold(III) chloride hydrate (99.999% trace metal basis, Acros Organics), hydrogen hexachloroplatinate(IV) hexahydrate (37.3–38.0% Pt basis, TCI), hexadecyltrimethylammonium bromide (CTAB, >98%, TCI), sodium borohydride (≥97%, Carl Roth), ascorbic acid (>99%, VWR), tetrabutylammonium borohydride (TBAB, 98%, Sigma-Aldrich). Ultrapure water (ELGA Purelab Classic UV, 18.2 MΩ cm^{-1} at 20 °C, below 3 ppb TOC) was used to prepare all aqueous solutions.

Synthesis of gold nanocubes

The cubic nanoparticles were synthesized in seed-mediated growth according to a literature protocol.[19,37] In the first step, seed particles were prepared. Therefore, 273.3 mg (0.75 mmol) of CTAB was dissolved in 7.7 mL ultrapure water. In another container, 0.25 mL ultrapure water was added to 1.0 mg (0.0025 mmol) of gold(III) chloride hydrate. For a stock solution, 3.0 mg (0.079 mmol) of sodium borohydride was dissolved in 8.0 mL ultrapure water. All solutions were sonicated for a few minutes. At a constant water bath temperature of 28 °C and under magnetic bar stirring, 0.6 mL of the freshly prepared sodium borohydride solution was immediately injected into the solution of CTAB and the gold(III) chloride hydrate solution. After stirring for 3 min, the reaction solution was stored for 1.5 h in a water bath at 28 °C.

For the growth step, 174.9 mg (0.48 mmol) of CTAB was dissolved in 9.6 mL, and 0.8 mg (0.002 mmol) gold(III) chloride hydrate was dissolved in 0.2 mL ultrapure water. A

third solution was prepared by dissolving 100.4 mg (0.57 mmol) of ascorbic acid in 0.95 mL ultrapure water. First, the ascorbic acid solution and then 5 μL of diluted seeds (1 mL of the seed dispersion and 9 mL ultrapure water) were injected into a mixture of CTAB and gold(III) chloride hydrate constantly stirred at 45 °C in an oil bath with a magnetic stir bar. After the injection, the reaction solution was stirred at 45 °C for further 30 s and then left undisturbed at this temperature for 20 min. For purification, the nanoparticle dispersion was centrifuged at 10 000*g* for 10 min. The particles were redispersed in 5 mL ultrapure water and then centrifuged again under the same conditions and stored for further utilization in 1 mL ultrapure water.

Synthesis of bimetallic nanoparticles

To synthesize the bimetallic nanocubes, 24.2 mg (0.066 mmol) of CTAB was dissolved in 4.5 mL ultrapure water. In another container, for a stock solution, 5.2 mg (0.01 mmol) of hydrogen hexachloroplatinate(IV) hexahydrate was dissolved in 1.0 mL ultrapure water. In a third container, a stock solution of ascorbic acid (for the dendritic structures) or TBAB (for the core–shell nanoparticles) was prepared. Therefore, 8.8 mg (0.05 mmol) of ascorbic acid was dissolved in 5.0 mL ultrapure water, or 2.7 mg (0.1 mmol) of TBAB was dissolved in 1.0 mL ultrapure water. At an oil bath temperature of 100 °C, 0.25 mL of the previously prepared gold nanocubes were injected into the CTAB solution. 50 μL of hexachloroplatinate(IV) hexahydrate and 85 μL of the reducing agent solution were added to this mixture. The solution was stirred at 100 °C for one hour before purification. For lower platinum coverage of the dendritic particles, 10 μL of the hexachloroplatinate(IV) hexahydrate and 17 μL of the ascorbic acid solution were used. They were centrifuged for 10 min at 10 000*g* to precipitate the nanostructures. Then the particles were dissolved in 2.5 mL ultrapure water and centrifuged under the same conditions again. For further investigations, the nanoparticles were stored in 0.5 mL ultrapure water.

Characterization

The nanocrystals were characterized by using electron microscopy. Therefore, a transmission electron microscope Zeiss 900 N was used, operating at 80 kV. High-resolution investigations were done with an aberration corrected high-resolution transmission electron microscope Jeol JEM-ARM200F NeoARM equipped with a cold field emission gun operated at 200 kV acceleration voltage. Images were taken with a high-angle annular dark field detector (HAADF) and EDS data were acquired using a Jeol detector with an active area of 100 mm^2. For sample preparation, a diluted nanoparticle solution was dropped on a Formvar/carbon-coated copper grid or on a Formvar/Lacey carbon-coated copper grid (Plano, 300 mesh) or on a Lacey carbon-coated copper grid with a single layer of graphene film (Micro to Nano, 300 mesh) and was dried for a few hours under ambient conditions. To analyze the electron microscopy data ImageJ 1.53t and Gatan Digital Micrograph 3.53.4031.2 were used.

UV/vis measurements were carried out with a double-beam spectrometer of type SPEKOL 2000 from Analytik Jena. The slit width for the measurements was 2 nm and the step size was 0.2 nm. Before measurement, the nanoparticle dispersion was diluted to avoid saturation.

Results and discussion

Characterization of monometallic gold nanocubes

For the preparation of the bimetallic gold–platinum nanostructures, gold nanocubes are used as seed particles. The overview TEM micrographs of these nanocrystals are presented in Fig. S1a and b.† The majority of the gold particles, approximately 72%, have a cubic particle shape. Furthermore, a minor proportion of spherical and nearly triangular particles, comprising less than 28% of the total, were observed. These results are in very good agreement with the results of a previous study.[19] The gold nanocubes have a narrow size distribution with an average particle size of (50.9 ± 1.4) nm (3%) and show a localized surface plasmon resonance (LSPR) at 538 nm in the UV/vis spectrum (Fig. S1c and d†). With a small relative standard deviation of 3%, the cubic particles can be classified as monodisperse.[38] Fig. 1a and b present an atomically-resolved high-angle annular dark-field scanning transmission electron microscopy (HAADF-STEM) image of a cubic gold nanoparticle, which enables a detailed view of the particle's structure. The first noticeable aspect is the cubic structure with rounded corners. The particles are single crystalline with a face-centered cubic (fcc) structure. From these images, an interplanar spacing of 2.05 Å was measured which is in good agreement with the Au(200) plane.[39] In addition, the fast Fourier transformation (FFT) pattern from the whole gold nanocube (Fig. 1c) confirms this result. Reflexes are visible corresponding to a lattice

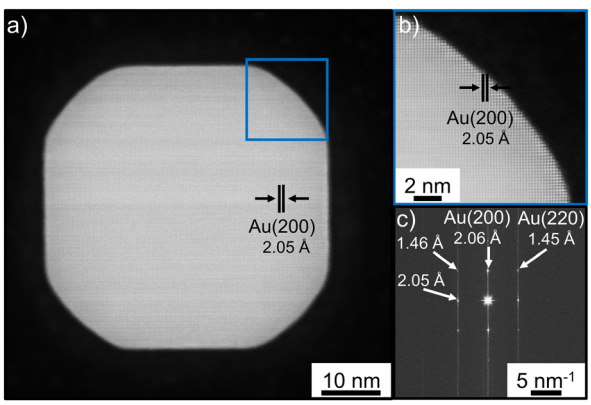

Fig. 1 a) HAADF STEM image of a gold nanocube with measured atomic distance. b) Section from the rounded corner of the gold nanocube with identical lattice parameter. c) FFT pattern of the whole gold nanocube with indicated lattice parameters for visible spots.

distance of 1.46 Å, 1.45 Å and 2.05 Å, 2.06 Å. These reflexes belong to Au(220) and Au(200) in accordance with the literature.[39,40]

Stability studies of the cubic gold nanocrystal revealed an instability of these nanostructures at higher temperatures of about 100 °C, the working temperature for the later bimetallic synthesis. Heat treatment results in the transformation of the cubes into spherical-appearing nanostructures, probably due to a ripening process (Fig. S2†). This was also observed in a previous study during a ligand exchange process in which the nanoparticle dispersion in oleylamine was heated up to 100 °C and a transformation to thermodynamically preferred shapes such as truncated octahedrons occurred.[19]

Characterization of the bimetallic nanoparticles

In the synthesis of bimetallic nanoparticles, some important parameters influence the size, shape, and structure of the resulting particles. This includes, for example, the particle-stabilizing ligand, the reaction temperature, the metal salt used, and the reducing agent. By exchanging the reducing agent from tetrabutylammonium borohydride (TBAB) to ascorbic acid, we were able to synthesize core–shell or dendritic nanostructures, respectively.

Gold–platinum core–shell nanocubes

Fig. 2a presents an overview TEM image of bimetallic gold–platinum nanostructures using tetrabutylammonium borohydride (TBAB) as a reduction agent for the platinum metal salt. Comparable to the monometallic gold nanocubes, most of the particles (about 70%) have a cubic shape. Besides, there is also a small amount of almost triangular and spherical-appearing particles, which is equivalent to the initial nanoparticles. The formation of sharper corners and additional tips on the previously rounded corners of the nanocubes are observed as a result of adding platinum. The particle size increases by about 1.5 nm from (50.9 ± 1.4) nm of the initial gold nanocubes to (52.6 ± 1.5) nm (3%) of the Au–Pt_{CS} nanocubes (Fig. S3†). In addition, some of the irregularly shaped nanoparticles showed a roughened surface and additionally grown tips (Fig. S4†). When the gold nanocubes are heated to 100 °C, a change in shape is observed. In contrast, the cubic shape of the bimetallic nanocrystals is retained, despite the synthesis occurring under comparable reaction conditions. This indicates the stabilization of the particles by the attachment of platinum. Similarly, the stabilization of palladium nanocubes was observed when attaching rhodium as reported by Gilroy and Lu *et al.*[22,41] They prepared palladium nanocubes that were unstable observed by *in situ* heating transmission electron microscopy, but the formation of palladium–rhodium core–frame nanocubes preserved the cubic morphology. As a result of the platinum attachment, a slight blueshift of the plasmon resonance by about 4 nm is observed in the UV/vis spectrum of the gold–platinum core–shell nanocubes (Fig. 2b) in combination with a broadening of the LSPR signal. In general, a broadening and damping of the LSPR signal is commonly observed when decorating gold nanoparticles with platinum.[42]

To verify the existence of platinum and to obtain more information about the elemental composition and distribution, energy-dispersive X-ray spectroscopy (EDS) was performed. The elemental maps in Fig. 3 indicate the presence of a core–shell structure of the analyzed dimer. The elemental distribution of gold (c), platinum (d), and a superimposed image of the distribution of gold and platinum (b) are shown related to the HAADF-STEM in (a). Please note that the distortion is an artifact due to a drift of the sample during the EDS mapping. In Fig. 3c, the elemental distribution of gold exhibits the typical cubic shape of the initial gold nanocubes. Platinum was detected as a shell around the cubic gold core and at the new tips formed at the previously rounded corners. The acquired EDS spectra are shown in Fig. S5 and S6.† The bimetallic nanocubes contain approximately 89% predominately gold and about 11% platinum as determined from the EDS data.

For a more detailed view of the particle structure, high-resolution TEM measurements were performed. The atomically-resolved HAADF-STEM image in Fig. 4a represents a section from a corner of an Au–Pt_{CS} nanocube and shows a single-crystal lattice with epitaxial growth of platinum on gold. The

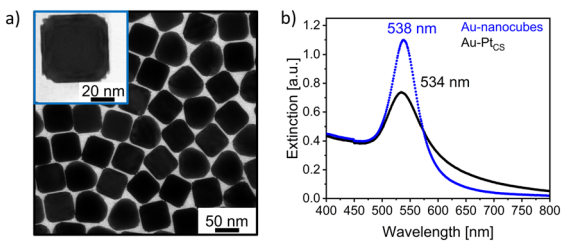

Fig. 2 a) TEM micrograph of gold–platinum nanoparticles synthesized with the reducing agent TBAB (inset: single nanoparticle to exhibit the formation of formed tips at the formerly round corners). b) UV/vis spectrum of the initial cubic gold nanoparticles (blue line) and gold–platinum core–shell nanocrystals (black line).

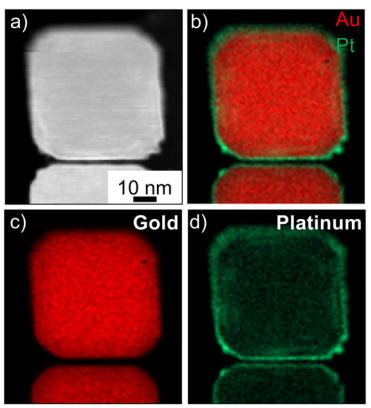

Fig. 3 a) HAADF-STEM image of cubic gold–platinum nanoparticles synthesized with TBAB as the reducing agent. b) Elemental distribution of gold and platinum, c) elemental distribution of gold Lα, and d) elemental distribution of platinum Lα.

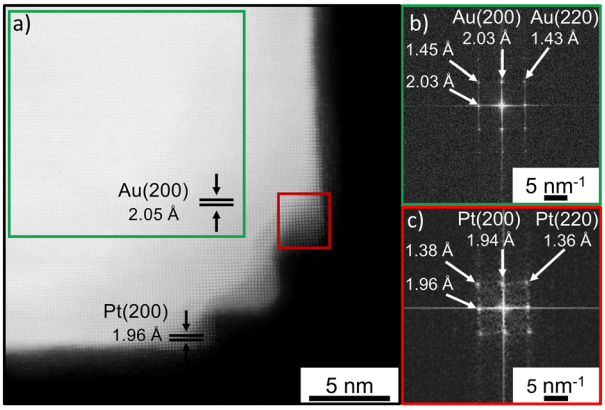

Fig. 4 a) HAADF STEM image of a section from a rounded corner of the Au–Pt_{CS} nanocube synthesized with the reducing agent TBAB. b) FFT pattern of the nanoparticle bulk region (green box). c) FFT pattern of a tip from the corner of this nanocube (red box).

corresponding FFTs are shown in Fig. 4b and c, respectively. The determined lattice constant in the cubic particle corpus is 2.05 Å (Au(200)[39,43]) and is the same as for the monometallic cubes. This indicates that the surface structure is not modified with the attachment of platinum. In contrast, an interplanar spacing of 1.96 Å was measured at the tips which is in accordance with Pt(200).[44] The results, confirm the core–shell structure of the nanoparticles observed in EDS mapping and show that a site-selective platinum overgrowth occurs due to the reaction conditions.

To investigate the influence of the amount of reducing agent and the quantity of platinum on growth, these parameters were varied. A reduction of the amount of the platinum precursor by 50% combined with the same amount of TBAB also results in the formation of cubic nanoparticles with additional peaks at the previously rounded corners (Fig. S7a†). Besides, growth tips were formed even, if the reducing agent and the amount of platinum metal salt were reduced by half (Fig. S7b†).

The particle growth can be presumed to have proceeded *via* layer-by-layer growth. In this process, the atoms chemisorb on the particle surface and then diffuse to energetically favored particle sites (*e.g.* corners and edges). Thus, the diffusion rate is higher than the deposition rate. The growth mechanism is partly controlled by the particle stabilizing ligand CTAB. Bromide preferentially chemisorbs onto the Au(100) facets and blocks them. Besides, the reaction temperature is a crucial factor in this process, as it influences the interaction between the specific facets and the mobility of the adatoms on the particle surface. This was previously demonstrated in a study on the synthesis of gold nanocubes.[19] Furthermore, the choice of reducing agent is also an important factor, as it allows for the precise control of monomer concentration, which can influence the growth mode and the final particle architecture.

Dendritic gold–platinum nanoparticles

The effect of varying the reduction agent in the synthesis of gold–platinum nanoparticles on the resulting particle

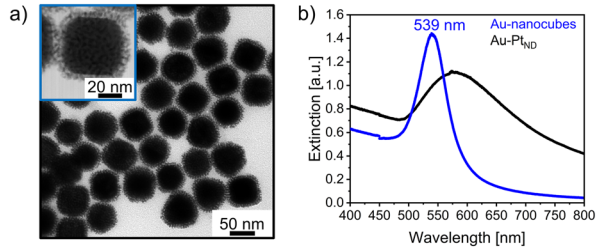

Fig. 5 a) TEM micrograph of dendritic gold–platinum nanoparticles synthesized with the reducing agent ascorbic acid. b) UV/vis spectrum of the initial cubic gold nanoparticles (blue line) and dendritic gold–platinum nanocrystals (black line).

architecture is presented in Fig. 5. The use of the reducing agent ascorbic acid instead of TBAB results in the formation of islands rather than the layer-by-layer growth mode. A highly branched, dendritic platinum shell of approximately 7 nm has formed on the surface of the gold nanocubes. Compared to the initial cubic gold seed particles, some nanocrystals seem to become slightly rounder, which will be discussed further below. Moreover, all nanoparticles exhibit a highly branched dendritic shell, regardless of the particle shape. The optical properties of the platinum nanocubes are modified by the addition of a dendritic platinum shell as a result of a change to the dielectric environment. As a result, the corresponding UV/vis spectrum in Fig. 5b exhibits a significant redshift in combination with a broadening of the LSPR signal. This is in accordance with the literature reporting that platinum can dampen the plasmon resonance.[25,45]

EDS mapping was used to analyze the composition of the particle, especially of the dendritic shell. Fig. 6a shows a HAADF-STEM image of a dendritic nanoparticle together with the EDS maps (full EDS spectra in Fig. S8†). The results indicate the presence of a cubic-shaped gold core with rounded corners, as for the monometallic seed particles, surrounded by a highly branched dendritic platinum shell. According to EDS analysis, the ratio of gold to platinum is approximately 75% to 25%.

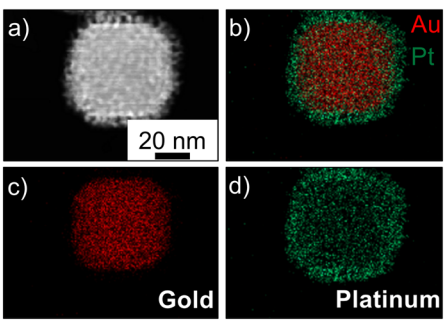

Fig. 6 a) HAADF-STEM image of a dendritic cubic gold–platinum nanoparticle synthesized with ascorbic acid as the reducing agent. b) Elemental distribution of gold and platinum, c) Elemental distribution of gold Lα, and d) Elemental distribution of platinum Lα.

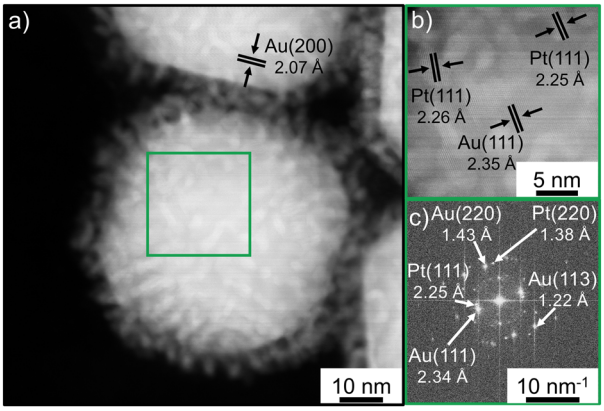

Fig. 7 a) HAADF STEM image of a gold–platinum nanoparticle with a dendritic shell, synthesized using ascorbic acid. b) Magnified section from the core region of the bimetallic particle (green box). c) FFT pattern of b.

In the corresponding HAADF image in Fig. 7a, the crystalline particle structure as well as the dendritic shell is visible. The magnified section from the core (Fig. 7b) shows the lattice spacing of gold and platinum. Fig. 7c also exhibits the presence of both metals due to the reflections corresponding to Au(111), Au(022), and Au(113) and Pt(111), Pt(220), and Pt(113).[46–50] These results confirm the presence of a gold core and a dendritic platinum shell of the particles. As previously noted, the shape of these bimetallic nanocubes appears to adopt a slightly rounded shape. This could be attributed to a different orientation of the nanoparticles on the TEM grid due to the dendritic shell. In comparison, the monometallic gold nanocubes and the core–shell nanocrystals show a preferred orientation on the TEM support. This is supported by the presence of particles having a cubic-shaped core and a lattice spacing of 2.07 Å that can be assigned to Au(200) (Fig. 7a).

The here reported syntheses of the bimetallic nanoparticles only differ by the use of the reducing agent for the platinum salt, otherwise keeping the solvent, ligands, additives, and reaction temperature and concentrations unchanged. The obtained results demonstrate that precise control of the architecture from the bimetallic nanoparticles is possible. By using reducing agents with different reduction strengths, the degree of supersaturation in the reaction solution is influenced and thus also the growth pathway,[51,52] resulting in the majority formation of dendritic nanostructures. The reducing potential of ascorbic acid appears to be dependent on temperature. If the synthesis is performed at 80 °C instead of 100 °C, this results in the formation of dendritic nanoparticles, which exhibit a much thinner platinum shell (Fig. S9†). Since the deposition rate for dendric particles is significantly increased compared to core–shell nanocrystals, it is apparent that the kinetics control the growth process of Pt islands. An island growth mode of platinum on various shapes of gold seed particles such as octahedra, rods, and triangular nanoprisms has been reported in the literature.[53,54] Based on the higher surface energy of platinum compared to gold and the lattice mismatch of 3.8% (ref. 55) between both metals, a preferential island growth of platinum on gold is known to occur.[26] Besides, the growth of islands will also be favored if the reaction temperatures are not sufficiently high, as diffusion of platinum monomers on a particle surface is hindered by the strong Pt–Pt bond.[22]

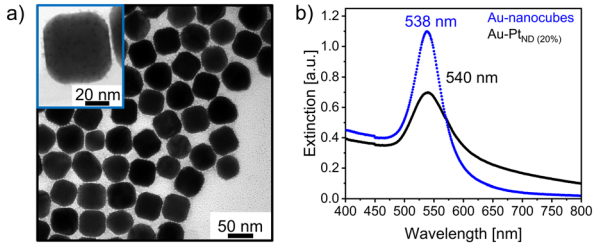

Fig. 8 a) Overview TEM micrograph of dendritic gold–platinum nanoparticles synthesized with 20% of the initial amount of platinum, but with the reducing agent ascorbic acid. b) UV/vis spectrum of the initial cubic gold nanoparticles (blue line) and dendritic gold–platinum nanocrystals (black line).

Dendritic gold–platinum nanoparticles with a lower platinum coverage

Fig. 8a illustrates the ability to modify the thickness of the dendritic platinum shell by varying the quantities of metal salt and the reducing agent ascorbic acid. The bimetallic particles exhibit isolated islands instead of a 7 nm dendritic shell due to the reduced amount of platinum precursor added (20% of the total metal salt reported in the previous section). Comparable to previously presented dendritic nanocrystals, the particle shape appears to be slightly rounded. In the recorded UV/vis spectra (Fig. 8b), the dendritic nanostructures show a slight redshift of approximately 2 nm and also a broadening of the LSPR signal.

The results obtained from EDS (Fig. 10) and high-resolution STEM (Fig. 9) measurements agree with the previously presented dendritic nanostructures. The elemental distribution in Fig. 10a presents a dendritic nanoparticle with isolated platinum islands grown on a cubic gold core (associated spectrum in Fig. S10†).

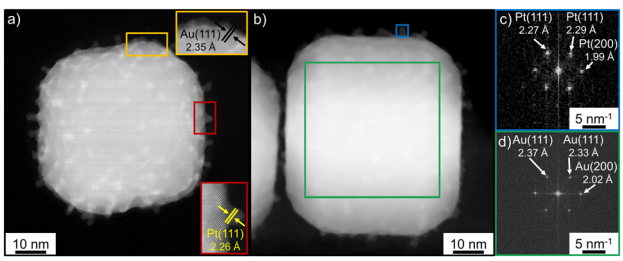

Fig. 9 a) HAADF STEM image of a dendritic gold–platinum nanoparticle synthesized with the reducing agent ascorbic acid. b) High-resolution HAADF-STEM image of another dendritic cubic gold–platinum nanoparticle in a different orientation on the TEM support. c) FFT pattern of a section of the dendritic shell (blue box). d) FFT pattern from the core region of the particle (green box).

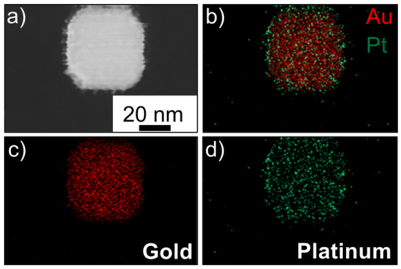

Fig. 10 a) HAADF-STEM image of a cubic gold–platinum nanoparticle synthesized with 20% of the initial amount of platinum, but with the reducing agent ascorbic acid. b) Elemental distribution of gold and platinum, c) elemental distribution of gold Lα, and d) elemental distribution of platinum Lα.

EDS analysis shows a gold–platinum ratio of 92% to 8%. These results are comparable to those of the previous core–shell structure, although a reduced quantity of platinum metal salt (20% of the previous amount) was used in the synthesis.

The high-resolution HAADF-STEM images in Fig. 9 show the crystalline structure of the dendritic nanoparticles. The results obtained for the dendritic nanoparticles with a dense shell and individual islands are comparable and in agreement with the EDS measurements. The lattice constant in the cubic particle corpus (Fig. 9a) is 2.35 Å (Au(111)) and the FFT of this area (Fig. 9d) only shows reflections belonging to gold. In contrast, the lattice spacing of the formed islands is 2.26 Å, which is assigned to Pt(111). In the corresponding FFT image (Fig. 9c), all reflexes can be assigned to platinum. These results confirm that the nanoparticle consists of a gold core and a platinum shell. As described above, the particles might be orientated differently on the TEM grid due to the platinum branches at the gold surface resulting in a variation of the projected shapes of the nanoparticles. Fig. 9a indicates a possible tilting of the nanoparticles because the edges no longer look like a straight line. Besides, an intensity gradient is visible in Fig. 9b. The particle appears brighter in the middle area compared to the top and bottom of the image. This directly shows that the particle is thicker in this area since the HAADF contrast scales with the thickness.[56,57] A linear proportionality of the HAAD-intensity to the sample thickness is known.[57]

By varying the amount of platinum used for the dendritic nanostructures, the density of platinum islands can be controlled as well as the optical properties, whereby higher platinum coverages lead to a broadening and redshift of the signal in the UV/vis spectrum. This can be useful for photocatalytic applications as with controlling the platinum coverage, the plasmon resonance can be influenced and tuned for the respective wavelength range of the solar spectrum.

Conclusion

In summary, this study demonstrates a controlling of the architecture of gold–platinum nanocubes due to the growth of platinum on gold nanocubes. This is achieved by the choice of the reduction agent, as this affects the reaction kinetics and thus the attachment of the platinum to the gold seeds. On the one hand, the reduction agent TBAB leads to the formation of core–shell nanoparticles with decorated rounded cube corners, exhibiting an epitaxial growth of platinum on gold. The instability of the gold nanocubes at temperatures around 100 °C at which the particles transform into the thermodynamically preferential spherical-appearing shape, presumably through a ripening process, is suppressed by the selective epitaxial growth of platinum on the gold nanocubes, indicating a stabilization by platinum. On the other hand, the use of ascorbic acid results in the growth of a dendritic structure. The particles have predominantly a cubic particle corpus. The different growth modes may be attributed to the different reduction strengths of the reducing agents and the degree of supersaturation. Based on the selected reaction conditions, the result indicates that ascorbic acid is a stronger reducing agent for the platinum metal salt than TBAB. Due to the different surface structures and attachments of platinum, the presented bimetallic nanocrystals have different surface-to-volume ratios. The UV/vis spectra indicate that the amount of Pt deposited, and the growth modus allow to tailor the optical properties. For example, high island densities broaden the absorbance by redshifting the spectrum while low island densities of similar crystallographic orientation mainly lead to damping of the plasmonic excitation with a minor redshift. On the other hand, similar Pt coverages but different growth modes and crystallographic orientations shift the absorption maximum differently. The question to be solved will be how those hybrid materials modify the scattering of the photons into the far field depending on the specific Pt growth. To summarize, cubic Au–Pt as an antenna–reactor system can be tailored according to specific needs with respect to catalytic and optical properties by a simple choice of reduction agent and thus is promising for aqueous photocatalytic applications.

Data availability

The data supporting this article have been included as part of the ESI.†

Author contributions

Imke Maack: conducting experiments (TEM, UV/vis), synthesis, data analysis & visualization, and writing manuscript. Kevin Oldenburg: HR-TEM measurements (together with Imke Maack), review & editing manuscript. Katharina Al-Shamery: conceptualization, project administration, supervision, funding acquisition, review & editing manuscript.

Conflicts of interest

There are no conflicts to declare.

Acknowledgements

The authors would like to thank Milena Osmiç for technical support in various TEM measurements. The Electron and Light Microscopy Service Unit of the Carl von Ossietzky University of Oldenburg is acknowledged for the use of the imaging facilities. The Deutsche Forschungsgemeinschaft (DFG, German Research Foundation) is gratefully acknowledged for funding the transmission electron microscope Jeol JEM-ARM200F NeoARM (DFG INST 264/161-1 FUGG).

Notes and references

1 M. S. Rider, Á. Buendía, D. R. Abujetas, P. A. Huidobro, J. A. Sánchez-Gil and V. Giannini, *ACS Photonics*, 2022, **9**, 1483.
2 W. Wang, M. Ramezani, A. I. Väkeväinen, P. Törmä, J. G. Rivas and T. W. Odom, *Mater. Today*, 2018, **21**, 303.
3 N. Nath and A. Chilkoti, *Anal. Chem.*, 2002, **74**, 504.
4 L. Olofsson, T. Rindzevicius, I. Pfeiffer, M. Käll and F. Höök, *Langmuir*, 2003, **19**, 10414.
5 N. Brinkmann, A. Damps, M. Siemer, J. Kräuter, F. Rößner and K. Al-Shamery, *J. Visualized Exp.*, 2022, **184**, e63936.
6 J. W. M. Crawley, I. E. Gow, N. Lawes, I. Kowalec, L. Kabalan, C. R. A. Catlow, A. J. Logsdail, S. H. Taylor, N. F. Dummer and G. J. Hutchings, *Chem. Rev.*, 2022, **122**, 6795.
7 P. Christopher, H. Xin and S. Linic, *Nat. Chem.*, 2011, **3**, 467.
8 T. T. Bich Quyen, W.-N. Su, C.-H. Chen, J. Rick, J.-Y. Liu and B.-J. Hwang, *J. Mater. Chem. B*, 2014, **2**, 5550.
9 Y. Sun and Y. Xia, *Science*, 2002, **298**, 2176.
10 S. Zhou, J. Li, K. D. Gilroy, J. Tao, C. Zhu, X. Yang, X. Sun and Y. Xia, *ACS Nano*, 2016, **10**, 9861.
11 W. Niu, L. Zhang and G. Xu, *ACS Nano*, 2010, **4**, 1987.
12 X. Hu, T. Wang and S. Dong, *J. Nanosci. Nanotechnol.*, 2006, **6**, 2056.
13 C. Wang, H. Daimon, Y. Lee, J. Kim and S. Sun, *J. Am. Chem. Soc.*, 2007, **129**, 6974.
14 C.-J. Huang, Y.-H. Wang, P.-H. Chiu, M.-C. Shih and T.-H. Meen, *Mater. Lett.*, 2006, **60**, 1896.
15 J.-E. Park, Y. Lee and J.-M. Nam, *Nano Lett.*, 2018, **18**, 6475.
16 S. Ghosh and L. Manna, *Chem. Rev.*, 2018, **118**, 7804.
17 M. Brown and B. J. Wiley, *Chem. Mater.*, 2020, **32**, 6410.
18 L. Mohrhusen and M. Osmić, *RSC Adv.*, 2017, **7**, 12897.
19 I. Maack, M. Osmić, L. Mohrhusen, P. Buhani and K. Al-Shamery, *ChemNanoMat*, 2021, **7**, 658.
20 M. Liu, K. D. Gilroy, H.-C. Peng, M. Chi, L. Guo and Y. Xia, *Chem. Commun.*, 2016, **52**, 13159.
21 Y. Xia, X. Xia and H.-C. Peng, *J. Am. Chem. Soc.*, 2015, **137**, 7947.
22 K. D. Gilroy, A. Ruditskiy, H.-C. Peng, D. Qin and Y. Xia, *Chem. Rev.*, 2016, **116**, 10414.
23 B. Lim and Y. Xia, *Angew. Chem., Int. Ed.*, 2011, **50**, 76.
24 X. Xia, S. Xie, M. Liu, H.-C. Peng, N. Lu, J. Wang, M. J. Kim and Y. Xia, *Proc. Natl. Acad. Sci. U. S. A.*, 2013, **110**, 6669.
25 S. Wang, N. Kristian, S. Jiang and X. Wang, *Nanotechnology*, 2009, **20**, 25605.
26 T. Bian, H. Zhang, Y. Jiang, C. Jin, J. Wu, H. Yang and D. Yang, *Nano Lett.*, 2015, **15**, 7808.
27 K. Qi, W. Zheng and X. Cui, *Nanoscale*, 2016, **8**, 1698.
28 N. Kohli, O. Singh and R. C. Singh, *Sens. Actuators, B*, 2011, **158**, 259.
29 B. Lim, H. Kobayashi, T. Yu, J. Wang, M. J. Kim, Z.-Y. Li, M. Rycenga and Y. Xia, *J. Am. Chem. Soc.*, 2010, **132**, 2506.
30 Z. Gao, H. Ye, D. Tang, J. Tao, S. Habibi, A. Minerick, D. Tang and X. Xia, *Nano Lett.*, 2017, **17**, 5572.
31 Y. Zhang, C. Lu, G. Zhao and Z. Wang, *RSC Adv.*, 2016, **6**, 51569.
32 U. Kreibig and M. Vollmer, *Optical Properties of Metal Clusters*, Springer-Verlag, Berlin, Germany, 1995.
33 A. Taketoshi and M. Haruta, *Chem. Lett.*, 2014, **43**, 380.
34 S. Linic, S. Chavez and R. Elias, *Nat. Mater.*, 2021, **20**, 916.
35 M. Muzzio, J. Li, Z. Yin, I. M. Delahunty, J. Xie and S. Sun, *Nanoscale*, 2019, **11**, 18946.
36 V. R. Stamenkovic, B. Fowler, B. S. Mun, G. Wang, P. N. Ross, C. A. Lucas and N. M. Markovic, *Science*, 2007, **315**, 493.
37 H.-Y. Ahn, H.-E. Lee, K. Jin and K. T. Nam, *J. Mater. Chem. C*, 2013, **1**, 6861.
38 J. Park, J. Joo, S. G. Kwon, Y. Jang and T. Hyeon, *Angew. Chem., Int. Ed.*, 2007, **46**, 4630.
39 M. Xue and Y. Tan, *Nanoscale*, 2014, **6**, 12500.
40 B. Pauwels, G. van Tendeloo, W. Bouwen, L. Theil Kuhn, P. Lievens, H. Lei and M. Hou, *Phys. Rev. B: Condens. Matter Mater. Phys.*, 2000, **62**, 10383.
41 N. Lu, J. Wang, S. Xie, Y. Xia and M. J. Kim, *Chem. Commun.*, 2013, **49**, 11806.
42 L. Feng, X. Wu, L. Ren, Y. Xiang, W. He, K. Zhang, W. Zhou and S. Xie, *Chem. – Eur. J.*, 2008, **14**, 9764.
43 C.-L. Lu, K. S. Prasad, H.-L. Wu, J. A. Ho and M. H. Huang, *J. Am. Chem. Soc.*, 2010, **132**, 14546.
44 S. I. Lim, I. Ojea-Jiménez, M. Varon, E. Casals, J. Arbiol and V. Puntes, *Nano Lett.*, 2010, **10**, 964.
45 Z. Xu, C. E. Carlton, L. F. Allard, Y. Shao-Horn and K. Hamad-Schifferli, *J. Phys. Chem. Lett.*, 2010, **1**, 2514.
46 L. Mohrhusen, N. Brinkmann, K. Obermann, K. H. Ng, E. C. Atata, J. Kräuter, M. Osmić, M. Grebien and K. Al-Shamery, *J. Phys. Chem. C*, 2022, **126**, 16690.
47 R. Devivaraprasad, R. Ramesh, N. Naresh, T. Kar, R. K. Singh and M. Neergat, *Langmuir*, 2014, **30**, 8995.
48 L. León Félix, J. A. H. Coaquira, M. A. R. Martínez, G. F. Goya, J. Mantilla, M. H. Sousa, L. d. L. S. Valladares, C. H. W. Barnes and P. C. Morais, *Sci. Rep.*, 2017, **7**, 41732.
49 J. W. Edington, in *Electron Diffraction in the Electron Microscope*, Palgrave, London, 1975.
50 B. Zhang, D. Wang, Y. Hou, S. Yang, X. H. Yang, J. H. Zhong, J. Liu, H. F. Wang, P. Hu, H. J. Zhao and H. G. Yang, *Sci. Rep.*, 2013, **3**, 1836.
51 D. Singha, N. Barman and K. Sahu, *J. Colloid Interface Sci.*, 2014, **413**, 37.
52 H.-Y. Wu, M. Liu and M. H. Huang, *J. Phys. Chem. B*, 2006, **110**, 19291.
53 Y. Kim, J. W. Hong, Y. W. Lee, M. Kim, D. Kim, W. S. Yun and S. W. Han, *Angew. Chem., Int. Ed.*, 2010, **49**, 10197.

54 R. K. Leary, A. Kumar, P. J. Straney, S. M. Collins, S. Yazdi, R. E. Dunin-Borkowski, P. A. Midgley, J. E. Millstone and E. Ringe, *J. Phys. Chem. C*, 2016, **120**, 20843.
55 F.-R. Fan, D.-Y. Liu, Y.-F. Wu, S. Duan, Z.-X. Xie, Z.-Y. Jiang and Z.-Q. Tian, *J. Am. Chem. Soc.*, 2008, **130**, 6949.
56 D. O. Klenov and S. Stemmer, *Ultramicroscopy*, 2006, **106**, 889.
57 D. T. Tran, I. P. Jones, J. A. Preece, R. L. Johnston, K. Deplanche and L. E. Macaskie, *Nanotechnology*, 2012, **23**, 55701.